Supplemental Materials:

Supplementary Dataset 1: Streamline counts. The excel file detailing the streamlines received at each of the cortical parcels (left and right combined) from the BF (all voxels)(n=173). Source data are provided with this paper (see Data Availability) and are also available at https://github.com/sudesnac/HumanBF-Connectivity/blob/main/data/Diff_streamline-counts_summed_seed-BASF_voxels.xlsx

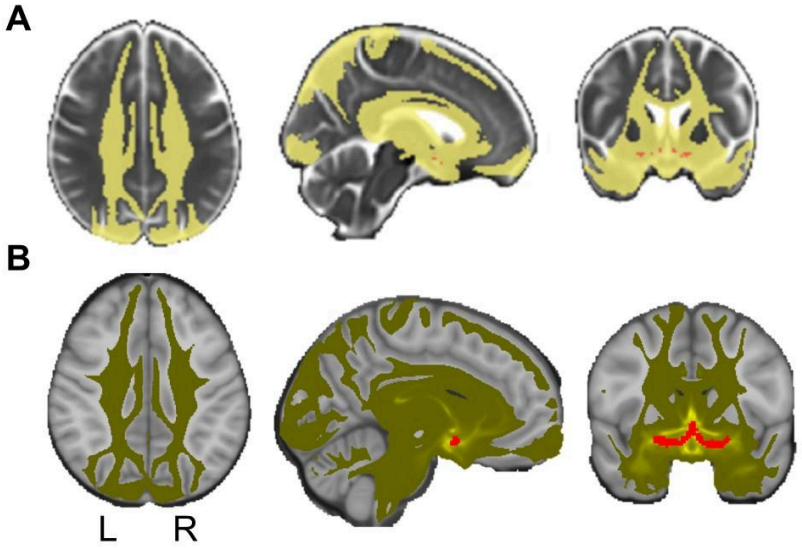

Supplemental Fig. 1: Basal forebrain (BF) cholinergic white matter pathways. (A) In vivo diffusion MRI tractography of the BF nucleus basalis of Meynert in a large sample of adults (n=262) adopted from Nemy et al.[1] Note that the medial and lateral tracts identified in vivo closely recapitulate the post-mortem tracing results as shown in Selden et al.[2] The image is reproduced with permission from Elsevier. (B) Diffusion tractography results from the present dataset (n=173). The strongest weighting corresponds to medial (cingulum) and lateral (capsular) BF pathways. See Supplementary dataset 1 and source data provided as a Source Data file for streamline counts.

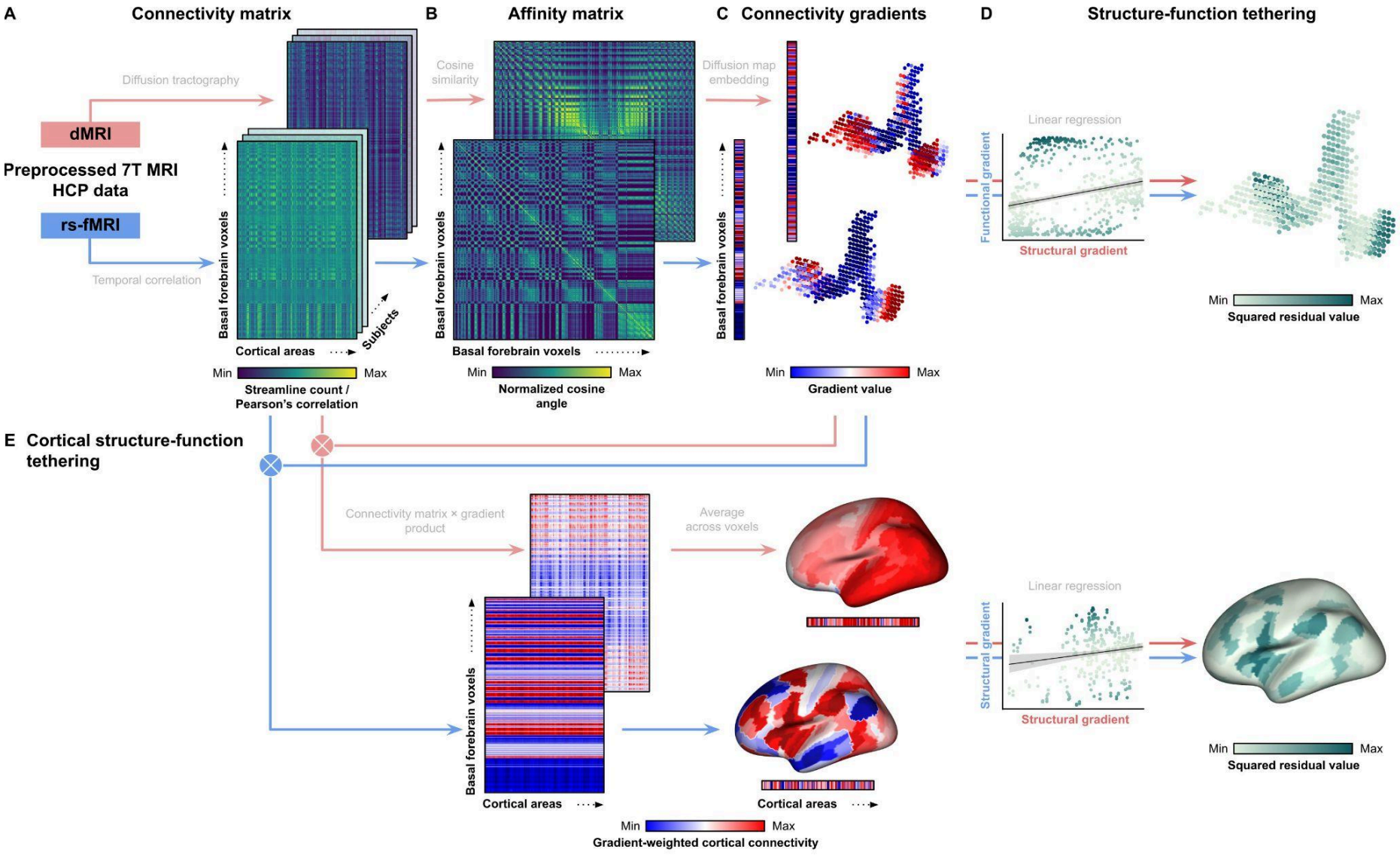
A
Connectivity matrix
Diffusion tractography
dMRI
Preprocessed 7T MRI
HCP data
rs-fMRI
Temporal correlation
Basal forebrain voxels
Cortical areas
Subjects
Min
Max
Streamline count /
Pearson's correlation
B
Affinity matrix
Cosine
similarity
Basal forebrain voxels
Basal forebrain voxels
Min
Max
Normalized cosine
angle
C
Connectivity gradients
Diffusion map
embedding
Basal forebrain voxels
Min
Max
Gradient value
D
Structure-function tethering
Linear regression
Functional gradient
Structural gradient
Min
Max
Squared residual value
E
Cortical structure-function
tethering
Connectivity matrix × gradient
product
Average
across voxels
Basal forebrain voxels
Cortical areas
Cortical areas
Min
Max
Gradient-weighted cortical connectivity
Linear regression
Structural gradient
Structural gradient
Min
Max
Squared residual value

Supplemental Fig. 2. Calculation of basal forebrain (BF) structure-function tethering. (A) Diffusion MRI (dMRI; red arrows) and resting-state fMRI (rs-fMRI; blue arrows) data (n=173) were processed separately to extract structural and functional connectivity matrices. dMRI data were used to reconstruct streamlines via diffusion tractography, while rs-fMRI data were analyzed for temporal correlations between BF voxels and cortical regions. (B-C) BF gradients were computed to demonstrate principal axes of connectivity variability among BF voxels, highlighting significant patterns based on inter-voxel similarity using the normalized cosine angle. (D) Linear regression was conducted between the first structural gradient (from streamline counts) and the first functional gradient (from Pearson's correlation strength) to derive voxel-wise residual values, measuring the degree of 'tethering'. (E) Gradient-weighted cortical maps were created by multiplying each row of the initial connectivity matrices with the corresponding principal gradient value, then averaging these rows to produce a single cortical representation of each gradient. Linear regression was then applied between the structural and functional gradient-weighted cortical maps to derive residual values for each cortical area.

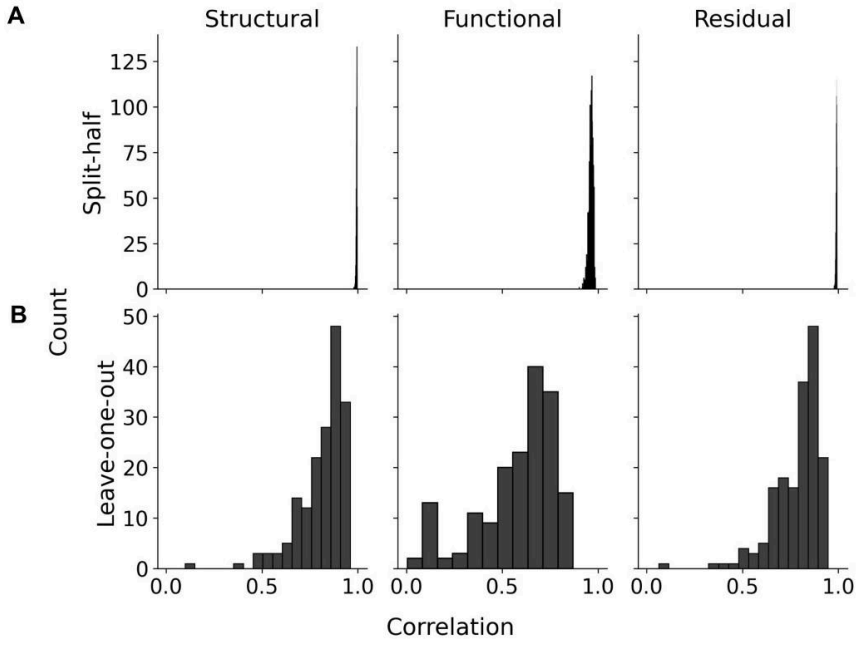

Supplemental Fig. 3. Calculation of split-half and leave-one-out cross-validation of basal forebrain (BF) gradients. (A) Split-half analysis: for each split (N=1000), the model was trained on the other half, and the predicted gradient was compared to the observed gradient for the left-out half. (B) Leave-one-out: for each subject left out (n=173), the model was trained on the remaining individuals, and the predicted gradient was compared to the observed gradient for the left-out individual. Source data are provided as a Source Data file.

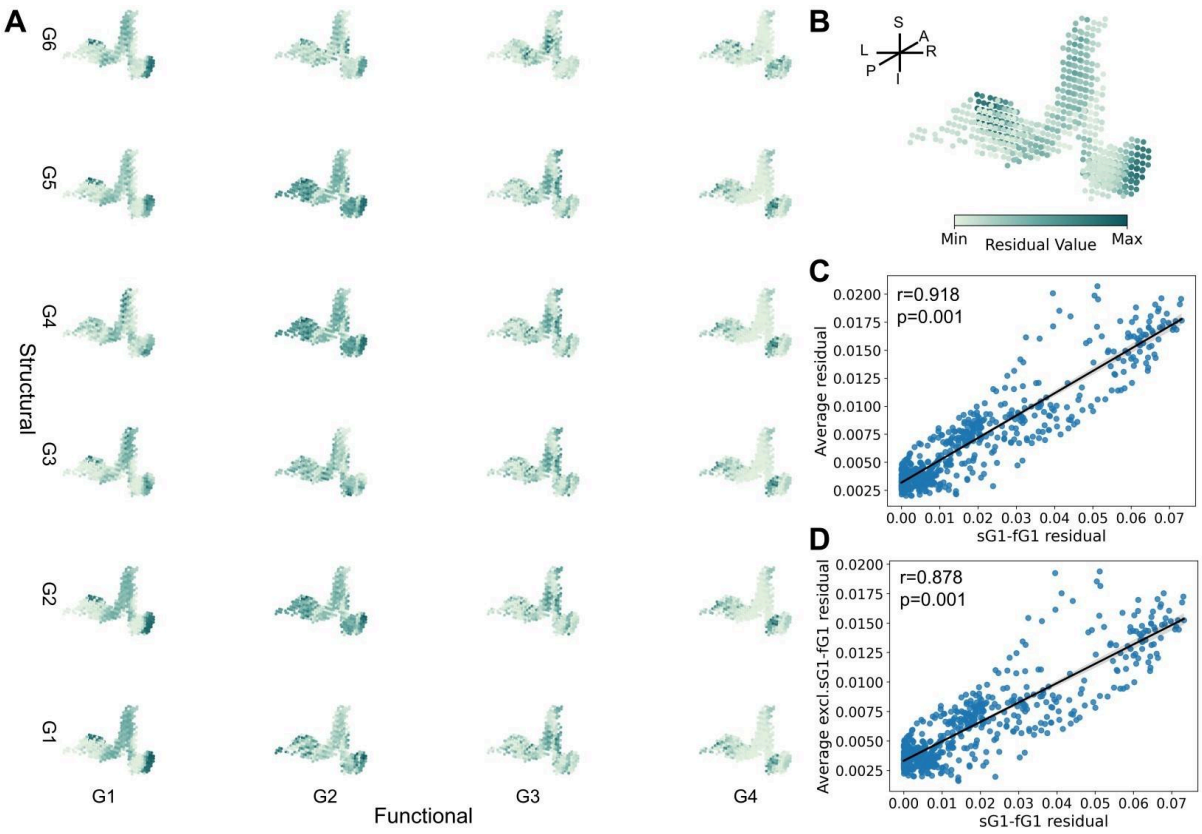

Supplemental Fig. 4. Calculation of structure-function tethering for all gradients falling above the knee points for their corresponding structural and functional gradients. (A) Residual BF for 24 structure-function gradient pairs: the knee-point[3] corresponded to sG6 for structural gradients and fG4 for functional gradients, thus forming 6 x 4 = 24 structure-function gradient pairs. (B) The average of the 24 residual maps qualitatively is highly similar to the sG1-fG1 residual map. (C) The Pearson's correlation between sG1-fG1 residual map (x-axis) and average of the 24 residual maps (y-axis). The solid line is the regression line. (D) The Pearson's correlation between sG1-fG1 residual map (x-axis) and average of the 23 residual maps, excluding sG1-fG1 residuals (y-axis). The solid line is the regression line. All source data are provided as a Source Data file.

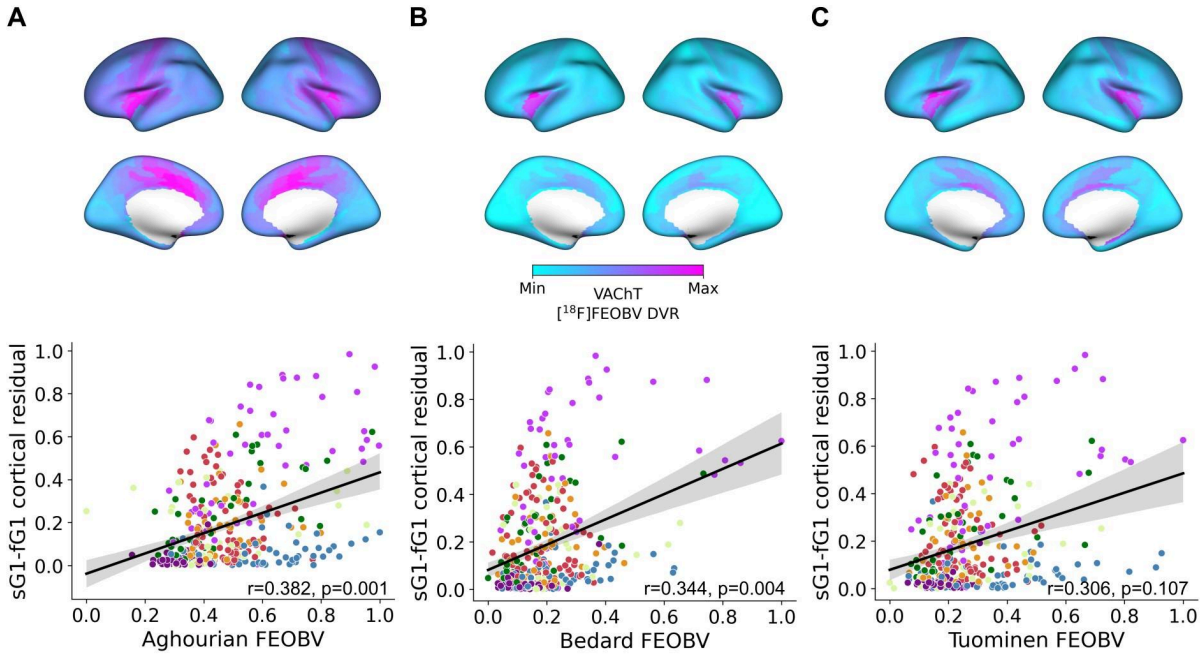

Supplemental Fig 5. Relation of basal forebrain (BF) structure-function tethering to three publicly available [^{18}F]FEOBV PET maps. (A) Aghourian et al[4] (B) Bedard et al.[5] (C) unpublished data provided to neuromaps by Tuominen et al.[6] Each point in the scatter plots represents cortical parcels based on HCP-MMP 1.0 parcellation color coded according to the Yeo networks[7] (Fig. 3B). Spin tests[8], as implemented in the neuromaps toolbox[6], were used to calculate Pearson's correlation and p-value based on N=10k permutation. The solid line is the regression line. The shaded area represents the size of the 95% confidence interval for the regression estimate, drawn as translucent bands around the regression line. The confidence interval is estimated using a non-parametric bootstrap procedure. Source data are provided as a Source Data file.

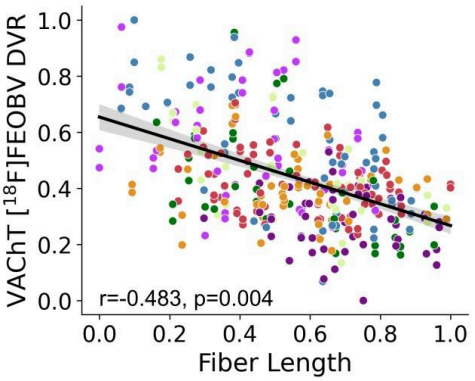

Supplemental Fig 6. Correlation of basal forebrain (BF) white matter fiber lengths to cortical [^{18}F]FEOBV PET binding (VAChT). Each point in the scatter plots represents cortical parcels based on HCP-MMP 1.0 parcellation color coded according to the Yeo networks[7] (Fig. 3B). Spin tests[8], as implemented in the neuromaps toolbox[6], were used to calculate Pearson's correlation and p-value based on N=10k permutation. The solid line is the regression line. The shaded area represents the size of the 95% confidence interval for the regression estimate, drawn as translucent bands around the regression line. The confidence interval is estimated using a non-parametric bootstrap procedure. Source data is provided as a Source Data file.

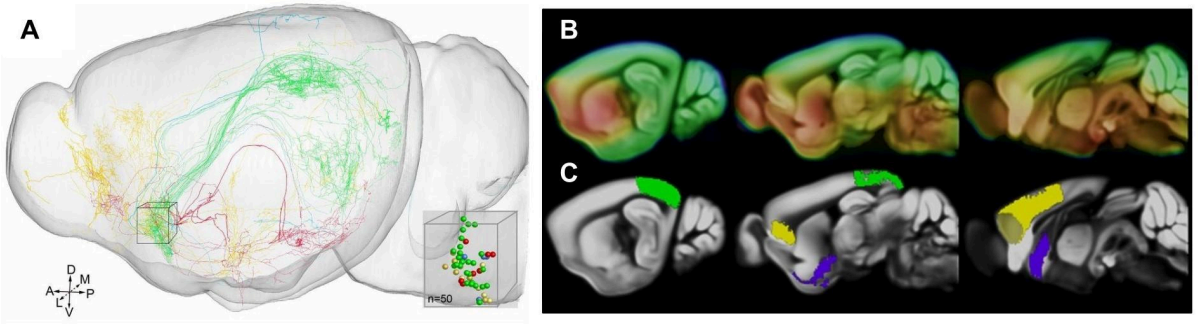

Supplemental Fig 7. Cellular labeling of cholinergic neurons in the mouse brain. (A) The half transparent sagittal view of the Allen Mouse Brain Atlas[9] is adapted from Li et al[10], showing axonal arborizations for 50 individual cholinergic neurons. The projections are color coded according to distinct anatomical locations they target. The soma of reconstructed neurons are shown in the 3D box inset with locations in medial septal nucleus and vertical band of Broca. (B) Average [^{18}F]FEOBV PET binding (V_T) in 11 wild type mice (VAChT$^{flox/flox}$; C57BL/6J) at 6 months of age in Allen Mouse Brain Atlas common coordinate framework (CCF) v3 reference space (sagittal view). (C) The Allen Mouse Brain Atlas CCF v3 annotations for the visual cortex (green) and salience network regions (yellow), including cingulate, infralimbic and orbitofrontal cortices. For reference, the BF nuclei (medial septal nucleus, diagonal band of Broca and substantia innominata) are labeled in purple.

Supplemental References

1. Reprinted from Nemy, M., Cedres, N., Grothe, M.J., Muehlboeck, J-S., Lindberg, O., Nedelska, Z., Stepankova, O., Vyslouzilova, L., Eriksdotter, M., Barroso, J., Teipel, S., Westman, E., & Ferreira, D. (2020). Fig. 3. Cholinergic WM pathways. In "Cholinergic white matter pathways make a stronger contribution to attention and memory in normal aging than cerebrovascular health and nucleus basalis of Meynert". NeuroImage, 211. https://doi.org/10.1016/j.neuroimage.2020.116607 with permission from Elsevier. Licensed under CC BY-NC-ND 4.0.
2. Selden, N. R., Gitelman, D. R., Salamon-Murayama, N., Parrish, T. B. & Mesulam, M.-M. Trajectories of cholinergic pathways within the cerebral hemispheres of the human brain. *Brain* **121**, 2249–2257 (1998).
3. Satopaa, V., Albrecht, J., Irwin, D. & Raghavan, B. Finding a ‘Kneedle’ in a Haystack: Detecting Knee Points in System Behavior. in *2011 31st International Conference on Distributed Computing Systems Workshops* 166–171 (IEEE, 2011).
4. Aghourian, M. *et al.* Quantification of brain cholinergic denervation in Alzheimer’s disease using PET imaging with [18F]-FEOBV. *Mol. Psychiatry* **11**, 1531–1538 (2017).
5. Bedard, M.-A. *et al.* Brain cholinergic alterations in idiopathic REM sleep behaviour disorder: a PET imaging study with 18F-FEOBV. *Sleep Med.* **58**, 35–41 (2019).
6. Markello, R. D. *et al.* neuromaps: structural and functional interpretation of brain maps. *Nat. Methods* **19**, 1472–1479 (2022).
7. Yeo, B. T. T. *et al.* The organization of the human cerebral cortex estimated by intrinsic functional connectivity. *J. Neurophysiol.* **106**, 1125–1165 (2011).
8. Alexander-Bloch, A. F. *et al.* On testing for spatial correspondence between maps of human brain structure and function. *Neuroimage* **178**, 540–551 (2018).
9. Kuan, L. *et al.* Neuroinformatics of the Allen Mouse Brain Connectivity Atlas. *Methods*

73, 4–17 (2015).

10. Li, A. *et al.* Generation of a whole-brain atlas for the cholinergic system and mesoscopic projectome analysis of basal forebrain cholinergic neurons. *Proceedings of the National Academy of Sciences* **115**, 415–420 (2017).